

Treatment of flue gas desulfurization wastewater by bipolar membrane electro dialysis and its optimization by response surface methodology

Ruiyuan Zhang^{a,*}, Yu Song^a, Yunpeng Li^a, Yaoqi Yang^a, Xuhui Sun^a, Yan Li^b

^aSchool of Chemistry Engineering, Northeast Electric Power University, Jilin 132012, Jilin, China,
email: zhangry2780@163.com (R. Zhang)

^bJilin Petrochemical Company Packaging Products Factory, Jilin 132022, Jilin, China

Received 6 November 2021; Accepted 23 July 2022

ABSTRACT

Flue gas desulfurization (FGD) wastewater is a terminal wastewater in power plant which seriously restricts the realization of zero-liquid discharge. Bipolar membrane electro dialysis (BMED) is a sustainable and eco-friendly technology widely applied in wastewater treatment. In this study, response surface methodology is employed to optimize the three key independent operating parameters: feed concentration, current density and initial acid and base concentration in order to increase desalination rate and by-product yield. The optimum condition was obtained as feed concentration 0.675 mol/L, current density 25 mA/cm² and initial acid and base concentration 0 mol/L. In this optimum condition, the mean value of alkali conversion rate could be higher than 89.99%. The process cost for the regeneration of 1 kg NaOH from the FGD wastewater was \$0.84. Increasing current density is an effective method to enhance by-product yield and shorten operation time, but it can cause a higher energy consumption, which means that the performance of the BMED system should be improved by optimizing operational conditions. Therefore, BMED is a new technology to realize the resource utilization and reuse of FGD wastewater.

Keywords: Flue gas desulfurization wastewater; Bipolar membrane electro dialysis; Response surface methodology; Process economy

1. Introduction

Coal, a major source of energy, is widely employed in coal-fired power plants (CFPPs) worldwide, especially in China. By the end of 2020, the installed capacity of CFPPs had been 1.08 billion kW, accounting for approximately 49.1% of the total installed capacity. Meanwhile, the CFPPs power generation accounted for 60.8% of the total. Limestone-gypsum wet flue gas desulfurization (FGD) technology has been used in more than 90% of CFPPs aiming for avoiding environmental pollution caused by SO₂ [1]. In order to maintain desulfurization efficiency and prevent equipment corrosion, the wet FGD technology is

necessary to discharge part of the FGD wastewater while controlling the chloride concentration to be less than 20,000 mg/L [2,3]. FGD wastewater has complex trait of high contents of suspended solids, heavy metals such as Hg, Cr, Pb and high chemical oxygen demand. In addition, the salinity content is at the range of 20–40 g/L, including large amounts of Ca²⁺, Mg²⁺, Cl⁻ and SO₄²⁻ [4]. In April 2015, Chinese government promulgated The Action Plan for Prevention and Treatment of Water Pollution [5,6]. This plan puts forward the requirement of zero-liquid discharge (ZLD), especially for FGD wastewater [7].

Early ZLD systems were based on thermal processes, where wastewater was typically evaporated in a brine

* Corresponding author.

concentrator followed by a brine crystallizer. The traditional brine concentrator are multi-effect distillation, mechanical vapor compression and multistage flash. These techniques are able to achieve high concentration brine but require high energy consumption. Subsequently, reverse osmosis (RO) and electrodialysis (ED) were incorporated into ZLD systems [8]. RO is a pressure-driven desalination technology that can raise the effluent salinity up to 70,000 mg/L. ED is applied to concentrate feed water to a high salinity ($\geq 100,000$ mg/L) with electric drive and ion exchange membranes [9]. RO and ED could reduce the volume of brine and improve energy and cost efficiencies. Recently, bypass evaporation tower and flue evaporation are utilized in CFPPs to realize ZLD. However, large-scale applications of these technologies are limited by the high operation costs and the reuse of solid inorganic salts [10]. As a consequence, it is necessary to find an appropriate FGD wastewater treatment technology to reduce the negative impact to environment.

Bipolar membrane electrodialysis (BMED) is a new membrane technique, utilizing the effect of direct-current electric field to dissociate H_2O into H^+ and OH^- , turning feed solution into corresponding acids and bases. BMED is widely used in organic acid production and recovery, heavy metals recovery, phosphate recovery, CO_2 capture, especially in wastewater treatment [11–14]. Herrero-Gonzalez et al. [15,16] and Chen et al. [17] utilized BMED to treat seawater reverse osmosis brine. Berkessa et al. [18] investigated the textile wastewater treatment by three-compartment BMED stack. Liu et al. [19] designed a novel BMED stack with multi-raffinate chambers disposing copper ore hydrometallurgical raffinate. Xia et al. [20] and Zhang et al. [21] used BMED to produce acids and bases from simulated FGD brine. Zhong et al. [22] reported a method of using selectrodialysis with the bipolar membrane to reuse coal chemical industry wastewater. Jiang et al. [23] combined RO, ED and BMED for salt recovery in the treatment of cold-rolling wastewater.

In this work, response surface methodology (RSM) with Box–Behnken design (BBD) was employed to establish a mathematical correlation involving feed concentration, current density and initial acid and base concentration and finally optimize these parameters in order to obtain the optimum operation condition and evaluate the process economy. The optimization of operation process will lay a foundation for treating FGD wastewater in electric power industry.

2. Experimental

2.1. Materials

FGD wastewater was provided by a CFPP located in Jilin Province, China. This raw water contains large amount of Cl^- and SO_4^{2-} with the molar ratio of 5:1. The concentration of simulated FGD wastewater used in the experiments was in the range of 0.45 to 0.75 mol/L, which was prepared with NaCl and Na_2SO_4 to control the fixed ratio. Membranes were provided by Kejia Polymer Materials Co., Ltd, Hefei, China. The characteristics of cation exchange membrane (CEM, CJMC-1), anion exchange membrane (AEM, CJMA-1) and bipolar membrane (BPM, CJBPM-1) are listed in Table 1. The reagents were analytical grade and provided by Sinopharm Chemical reagent Co., Ltd., China.

2.2. Experimental set-up

BMED apparatus used in the experiments was a BPM-AEM-CEM-BPM namely three-compartment system shown in Fig. 1, which was provided by Kejia Polymer Materials Co., Ltd., Hefei, China. The BMED stack was composed of two polarizing electrodes and five repeating units. The unit was separated by a 0.80 mm silicone partition nets and spacers, which constituted a salt compartment, an acid compartment and a base compartment. It can be observed from Fig. 1 that the simulated FGD wastewater, acid solution, base solution and electrolyte rinse solution were circulated in the stack driving by four peristaltic pumps, respectively. The cathode and anode were made of titanium plated with ruthenium. Each ion exchange membrane had an effective surface area of 189 cm^2 . All solutions should be circulated in each compartment for at least 20 min in order to eliminate the visible bubbles before applying current to BMED stack.

2.3. Analytical methods

The concentration of acid and base produced by BMED was determined by acid–base titration, using phenolphthalein and methyl orange as indicator, respectively. The voltage and current across the stack were recorded by a CV/CC regulated power supply (LONGWEI, TPR3020-2D). The conductivity and pH of simulated wastewater in salt compartment were measured during the entire process by conductivity meter (LEICI, DDS307A) and pH meter (METTLER

Table 1
Characteristics of membranes used for BMED stack

Items	Membranes		
	CEM	AEM	BPM
Type	Homogeneous	Homogeneous	Homogeneous
Functional group	Sulfonic acid	Quaternary amine	/
Thickness (μm)	140~150	90~100	150~180
Water content (%)	35~40	15~20	45~55
Ion-exchange capacity (meq/g)	0.8~1.0	0.8~1.0	/
Electric resistance (Ω/cm^2)	1.5~2.5	2.5~3.5	/
Transport number (%)	>98	>94	/

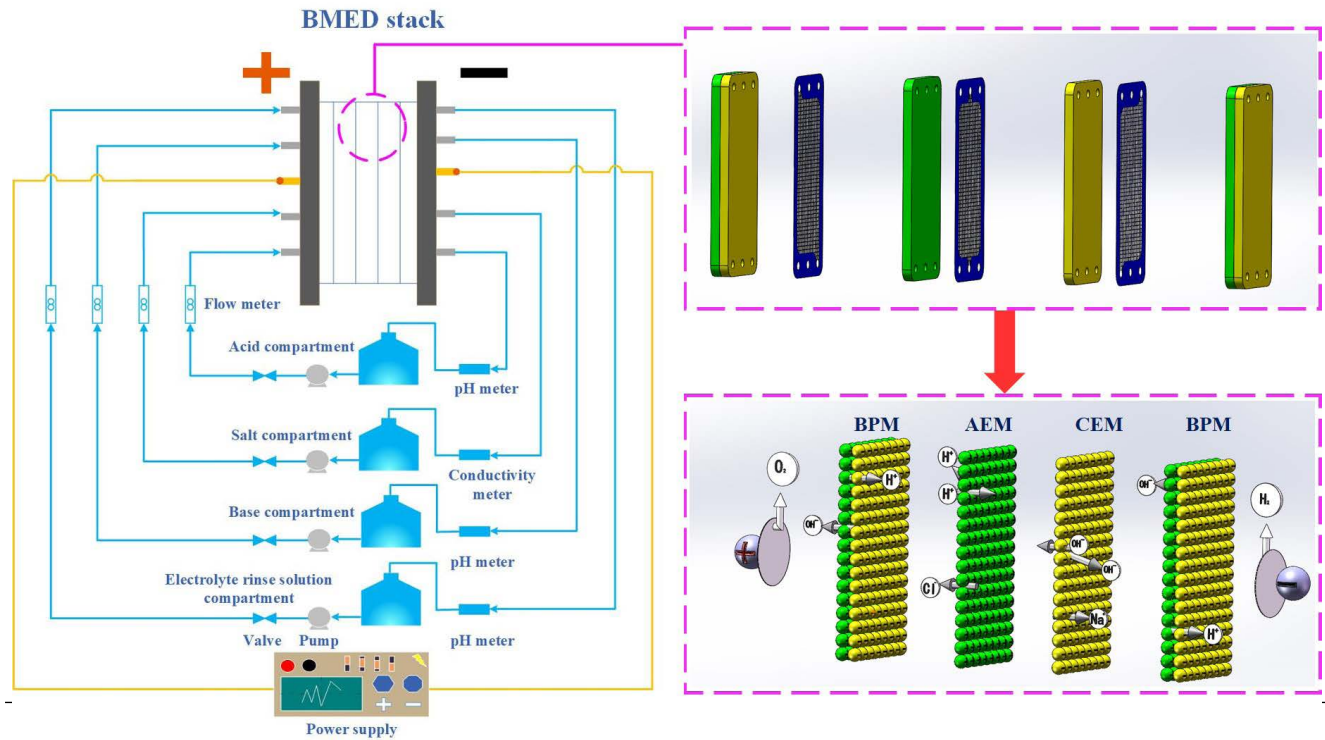


Fig. 1. Schematic diagram of the BMED apparatus and membrane stack.

TOLEDO, FE28), respectively. Morphology of layers on fresh and fouling membrane were observed by scanning electron microscope (SEM) (Hitachi SU8010, Japan). The samples were prepared before SEM imaging by coating with a thin layer of gold in order to reduce membrane surface charge. Fourier-transform infrared spectroscopy (FTIR) (IRAffinity-1, Japan) was used to analyze the change of functional groups on fresh and fouling membranes.

2.4. Determination of current efficiency and energy consumption

The current efficiency η (%) was calculated by Eq. (1).

$$\eta(\%) = \frac{zF(C_t V_t - C_0 V_0)}{60NIt} \times 100 \tag{1}$$

where z is the ion valence. F is the Faraday constant (96,500 C/mol). C_t and C_0 (mol/L) are the concentration of acid or base at time t and 0, respectively. V_t and V_0 (L) are the volume of acid or base solutions at time t and 0, respectively. N is the number of repeating units of the stack ($N = 5$). I is the current in the stack (A) and t is the operation time (min).

The energy consumption E (kWh/kg) was calculated by Eq. (2).

$$E = \int_0^t \frac{U_t Idt}{60(C_t V_t - C_0 V_0)M} \tag{2}$$

where U_t is the voltage drop (V) across the membrane stack at time t . M is the molar mass (g/mol) of the acid or base.

The alkali conversion rate ($X\%$) was calculated by Eq. (3).

$$X\% = \frac{(C_t V_t - C_0 V_0)M}{m} \times 100 \tag{3}$$

where m (g) is the initial weight of Na^+ in the salt compartment.

2.5. Experimental design

Response surface methodology is a combination of mathematical and statistical techniques based on the fit of a polynomial equation to the experimental data. This method could establish the interactive effects on BMED performance and to predict BMED performance. RSM is widely used in chemistry, biology and engineering disciplines [24–26]. Box–Behnken design is a factorial combination of at least three factors in incomplete blocks. In each block, one factor is held at the central point while the other two are varied in four different combination values at the upper and lower limits. RSM and BBD were employed to investigate the effects of the three independent variables on the response function. The independent variables were feed concentration (A), current density (B) and initial acid and base concentration (C). In order to obtain the optimum operational condition, two dependent parameters (alkali conversion rate and energy consumption) were analyzed as responses. The low, center, and high levels of each variable are designed as -1 , 0 , $+1$, respectively. Table 2 illustrates the variable factors with the code and actual values.

Experiments data from Box–Behnken design were represented employing a second-order polynomial models as follows:

Table 2
Experimental range and levels of the independent variables

Factors	Symbol	Coded levels		
		-1	0	1
Feed concentration (mol/L)	A	0.525	0.6	0.675
Current density (mA/cm ²)	B	25	30	35
Initial acid and base concentration (mol/L)	C	0	0.05	0.1

$$Y = \beta_0 + \sum_{j=1}^k \beta_j X_j + \sum_{j=1}^k \beta_{jj} X_j^2 + \sum_{i < j} \beta_{ij} X_i X_j + e_i \quad (4)$$

where Y is the estimated response variable, X_i ($i = 1, 2, 3$) and X_j ($j = 1, 2, 3$) represent the code independent variables, β_0 is a constant coefficient, β_j , β_{jj} and β_{ij} are interaction coefficients of linear, quadratic and the second-order terms, respectively, k is the number of studied factors and e_i is the error.

3. Results and discussion

3.1. Single-factor experiments

3.1.1. Effects of feed concentration

Fig. 2 indicates the results of BMED experiments at various feed concentrations when controlling the current density and flow rate at 30 mA/cm² and 30 L/h, respectively. The voltage drop curves across the BMED stack are shown in Fig. 2a. During the electrodialysis process, the voltage drop decreased at the initial stage of the experiment, reached an apparent minimum and then gradually increased. The main reason of high voltage drop was the high membrane stack resistance caused by the low concentration of acid and base in acid and base compartments. This is in agreement with values reported in literature by other authors [27–29]. As a consequence, it is easy to modify the performance of BMED system by changing the initial concentration of acid and base in the corresponding compartments which will be discussed in Section 3.1.3. The initial decreasing voltage drop could be ascribed to the progress of water splitting and ion migration in each compartment, which decreased the electrical resistance of the BMED stack [30]. Subsequently, the voltage drop maintained in a stable state, especially in high concentration. This phenomenon was a synergistic effect of the depletion of simulated wastewater and the production of acid and base. The conductivity of simulated wastewater in salt compartment decreased gradually to less than 10 mS/cm (Fig. 2b), suggesting that the solution was almost depleted and the resistance increase. Meanwhile, the production of acid and base decreased the resistance and maintain the resistance of BMED system at constant value. In the later stage of the experiment, the depletion of simulated wastewater was dominant and the voltage drop curve sharply increased. Fig. 2c shows the alkali conversion rate in different feed concentrations. It is clear the higher concentration of feed solution, the more ions could transport through the membranes at the same time, which was favor to produce higher concentration of

acid and base. The base concentration was 0.68 mol/L and corresponding alkali conversion rate was 77.89% when the simulated wastewater concentration is 0.75 mol/L. Fig. 2d depicts the effect of feed concentrations on current efficiency and energy consumption. It was found that enhance initial feed concentration led to the increase of current efficiency and the reduction of energy consumption. The current efficiency and energy consumption at feed concentration 0.675 mol/L were 75.96% and 2.24 kWh/kg, respectively. However, too high concentration is easy to cause a slight decrease in current efficiency.

3.1.2. Effects of current density

The effects of current density on voltage drop, base concentration and energy consumption were examined in the BMED system with 0.6 mol/L simulated wastewater at flow rate 30 L/h and different current densities (20–40 mA/cm²). The voltage drop across the BMED stack was a U shape as shown in Fig. 3a. The higher current density could result in higher voltage drop and shorter operation time, while the diffusion of ions were reduced between the adjacent compartments of BMED stack. Fig. 3b shows the base concentration and energy consumption as a function of current density at 20 min. It was observed that the higher current density enhanced the base concentration. According to the second Wien effect, the water splitting by bipolar membrane and ion transport through the membrane were increased simultaneously [31,32]. However, the energy consumption was proportional to the current density which could be ascribed to the fact that large amount of energy was used to overcome the electrical resistance at high current densities [33]. Accordingly, the selection of current density should be considered comprehensively. It is necessary to consider both the increased energy consumption caused by high current density and the prolonged reaction time caused by low current density, especially the product is volatile [27].

3.1.3. Effects of initial acid and base concentration

In order to reduce the resistance of BMED stack, the initial concentration of acid and base solution was modified at the range of 0–0.2 mol/L while current density, flow rate and feed concentration were controlled at 30 mA/cm², 30 L/h and 0.6 mol/L, respectively. Fig. 4a illustrates that the higher initial concentration of acid and base benefited to enhance the final concentration. The current efficiency and energy consumption are shown in Fig. 4b. The current efficiency decreases with the increase of the initial

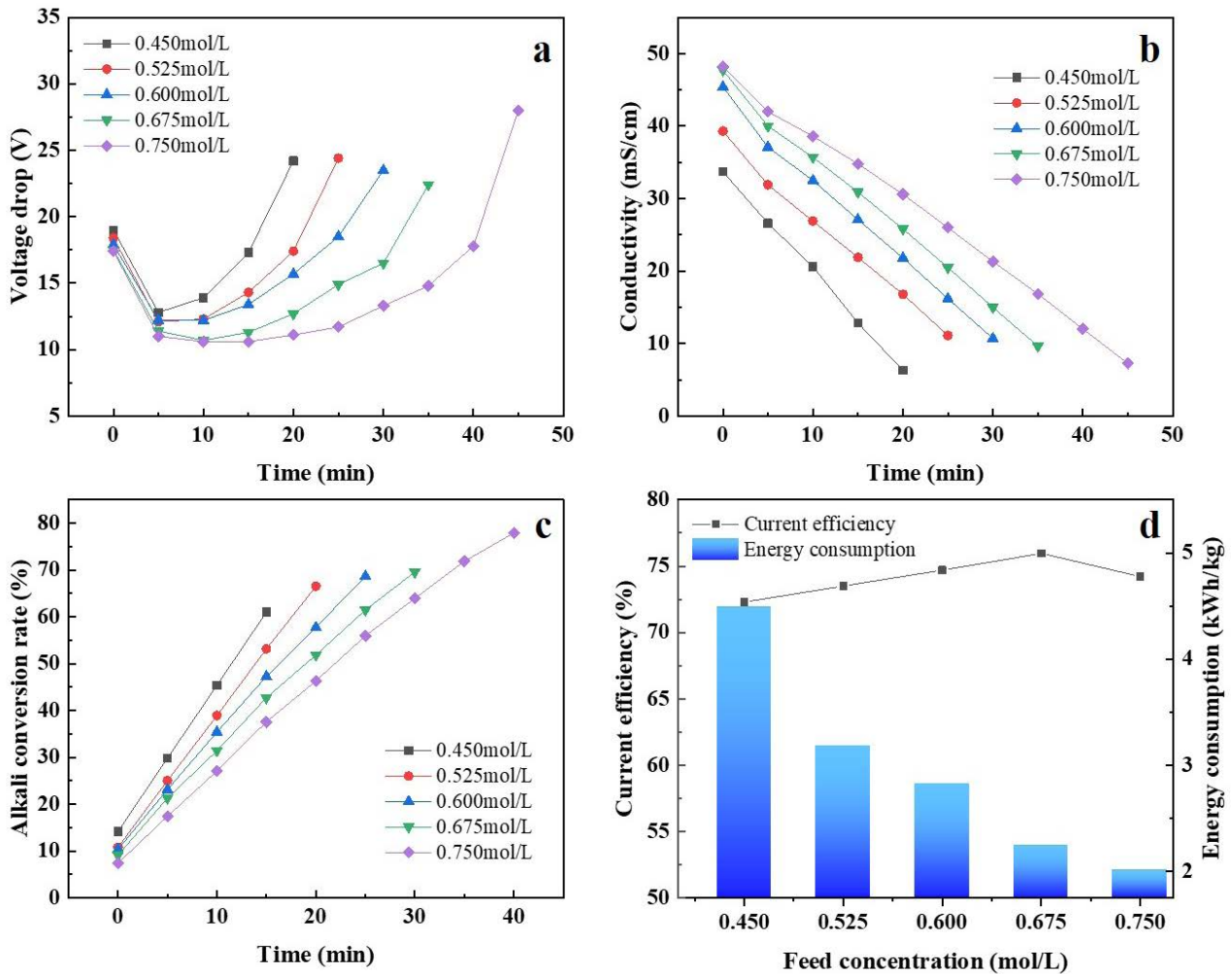


Fig. 2. Effects of feed concentration on (a) voltage drop, (b) conductivity, (c) alkali conversion rate, and (d) current efficiency and energy consumption.

concentration of the acid and base solution, which was mainly caused by the transfer resistance from salt compartment to acid and base compartments [34,35]. The energy consumption decreased firstly and then increased while reached the minimum at the initial concentration 0.05 mol/L. Appropriately increasing the initial acid and base concentration is beneficial to reduce the solution resistance and promote the electrolysis reaction, thereby increasing the acid and base production. However, when the concentration is too high, the diffusion of hydrogen ions or hydroxide ions from the acid compartment or the base compartment to the salt compartment will be increased due to the excessive chemical potential difference. The energy consumption will also increase if the concentration is too high.

3.2. Response surface Box–Behnken analysis

3.2.1. Analysis of variance

The analysis of variance (ANOVA) for regression parameters of the predicted response surface quadratic model

for conversion rate is shown in Table 3. The F -value was 53.29 and the probability value ($P_{\text{model}} < 0.0001$) were sufficient to indicate that the model was well adapted to the response. The lack of fit ($P = 0.1939 > 0.05$) is not significant, which is good for the model. Furthermore, the modeling was evaluated by the determination coefficient (R^2) and the adjusted determination coefficient (R_{adj}^2). In this study, the obtained value of R^2 ($R^2 = 0.9856$) indicated that more than 98.56% of the variability could be explained by the model. The value of R_{adj}^2 ($R_{\text{adj}}^2 = 0.9671$) disclosed a high significance of obtained model. Therefore, feed concentration (A), current density (B), initial acid and base concentration (C), interaction of AC and A^2 are the significant model terms, whereas other model terms can be considered insignificant. Two second-order polynomial models, using Design-Expert 8 software, in terms of coded factors are shown in Eq. (5).

$$y = 72.08 + 7.04 \times A - 5.50 \times B - 3.36 \times C - 1.10 \times AB - 2.40 \times AC - 1.41 \times BC + 1.98 \times A^2 + 0.78 \times B^2 + 0.52 \times C^2 \quad (5)$$

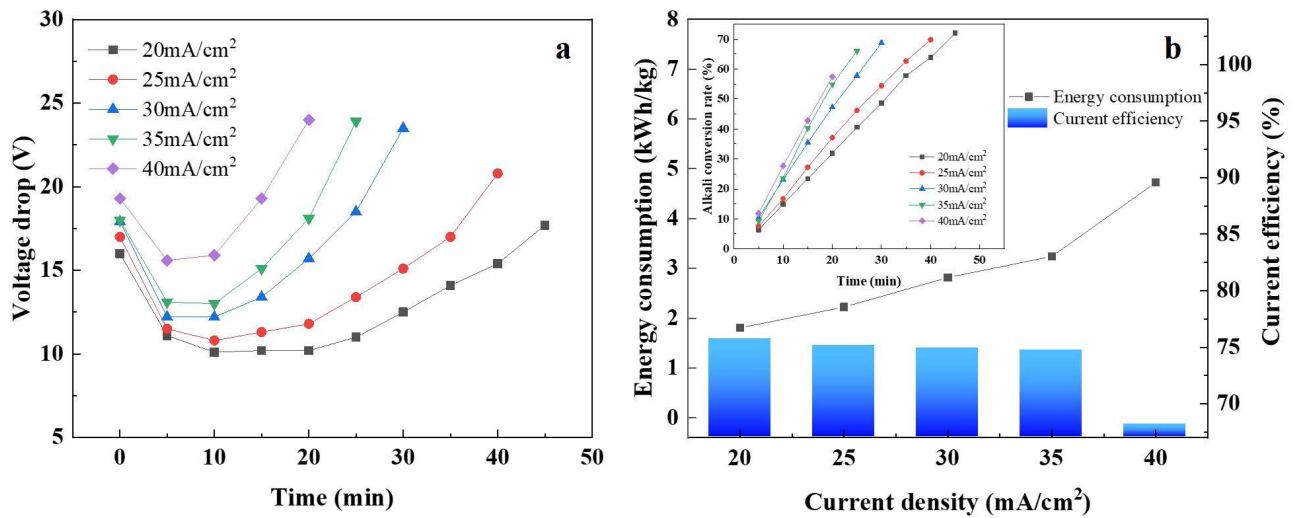


Fig. 3. Effects of current density on (a) voltage drop and (b) base concentration, current efficiency and energy consumption.

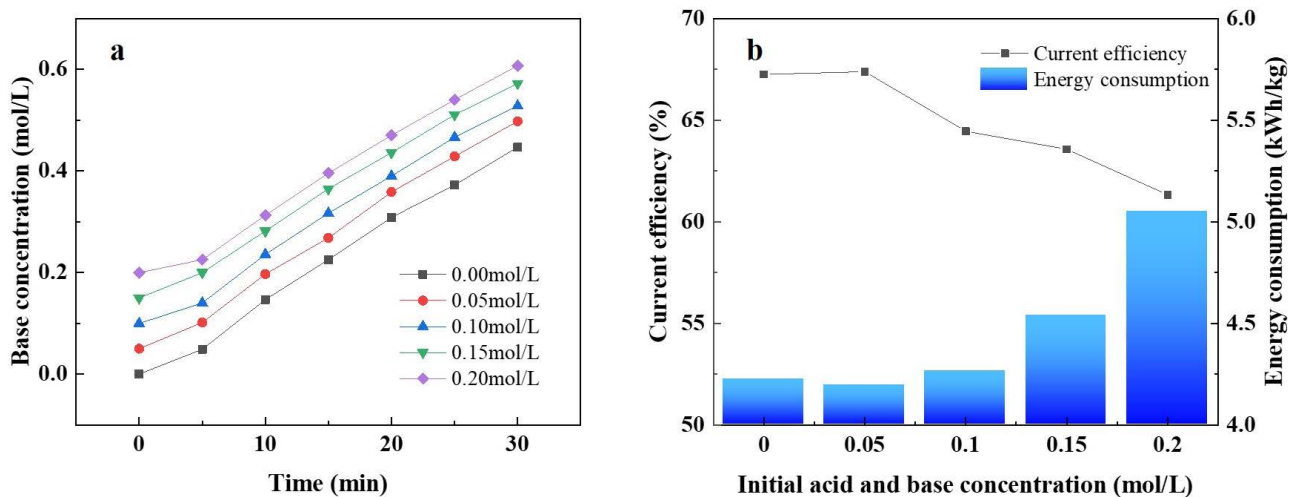


Fig. 4. Effects of initial acid and base concentration on (a) base concentration and (b) current efficiency and energy consumption.

Fig. 5 and Table 3 confirm a satisfactory correlation between the experimental and predicted values of alkali conversion rate. The points cluster along the diagonal line, which indicates that the model developed in this study was reasonably accurate.

3.2.2. Interaction effect and optimization

The three dimensional (3D) response surface graphs of the quadratic model were utilized to assess the interactive effects of the independent variables on the response. According to the *p*-value and 3D response surface graphs, the effect of feed concentration on the alkali conversion rate was more significant than that of current density and initial acid and base concentration. Fig. 6a shows the interaction between feed concentration and current density on alkali conversion rate. It is observed that higher feed concentration corresponds to higher alkali conversion rate.

The effects of current density and initial acid and base concentration on alkali conversion rate are shown in Fig. 6b. From the 3D graphs, increasing current density resulted in the decrease of alkali conversion rate when keeping initial acid and base concentration constant. Fig. 6c depicts the tendency of energy consumption with current density and initial acid and base concentration. The energy consumption was decreased with the initial acid and base concentration and reached a minimum in the range of 0.04–0.06 mol/L. Increasing current density was accompanied by the increase of energy consumption which was consistent with the single-factor experiment.

In numerical optimization performed by Design-Expert program, the optimum operation condition was considered. The results of numerical optimization were feed concentration 0.675 mol/L, current density 25 mA/cm² and initial acid and base concentration 0 mol/L, and the alkali conversion rate provided by the model under these

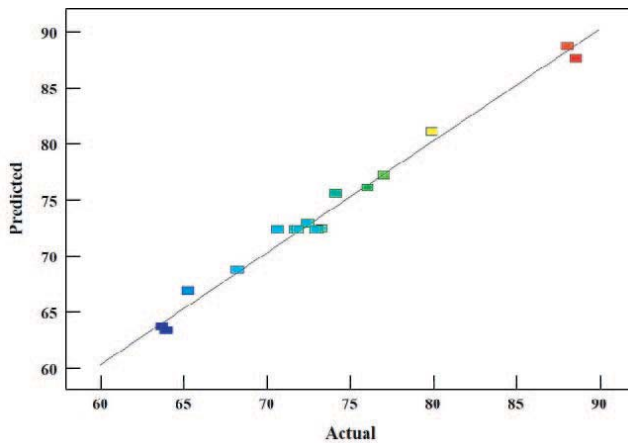


Fig. 5. Comparison between actual values and predicted values.

conditions was 93.36%. Experiments were implemented using the predicted optimum conditions in order to validate the developed mathematical models. The mean value of the alkali conversion rate was 89.99%, which were in close alignment with the predicted value. It is obvious that the model is adequate for the prediction of the alkali conversion rate.

3.3. Membrane surface fouling analysis

The fouling on membrane surface was identified by SEM and FTIR. As shown in Fig. 7a and c, the fresh AEM and CEM presented clean surfaces. After BMED process, no noticeable fouling deposits were observed on the surface of AEM and CEM as show in Fig. 7b and d. Fig. 7e and f show the FTIR spectra of fresh and fouling membranes. There is no obvious change except the decrease of some peak intensity.

3.4. Process economy

The operating cost was estimated on the basis of the above laboratory experimental equipment under a current density of 25 mA/cm² and feed concentration of 0.675 mol/L. The total cost of electro dialysis process based on the economy estimation routine contained the total investment cost and energy consumption [36–38]. The total investment cost consisted of stack cost and peripheral equipment cost. The cost of stack and peripheral equipment was proportional to the membrane cost and the cost of pumps, monitoring, control panels, etc, which were estimated to be 1.5 times total membrane cost and stack cost, respectively [39]. Both membrane lifespan and peripheral equipment amortization period were 3 y. Meanwhile, the estimate values of maintenance cost and interest were 10% and 8% of the total investment cost. The calculation results are shown in Table 4. It was clearly observed that the investment cost and energy consumption cost for producing base were \$236.50/y and \$0.13/kg, respectively. The process cost for the regeneration of 1 kg NaOH from FGD wastewater was \$0.84 which was lower than that in spent caustic regeneration [36]. Meanwhile, the total process cost could be reduced in pilot scale or industrial scale and made BMED technology more appropriate and competitive to treat FGD wastewater.

4. Conclusions

The Box–Behnken experimental design was proven to be a suitable response surface method to determine the effects of operative variables (feed concentration, current density and initial acid and base concentration) and their interaction on alkali conversion rate and energy consumption. The ANOVA indicated that the quadratic model and interaction were significant. The model fitted well with the experimental data, as confirmed by the high R^2 value. The optimal values for the three factors were feed concentration

Table 3
Analysis of variance result for significant model terms

Source	Sum of squares	df	Mean square	F-value	p-value Prob. > F
Model	787.25	9	87.47	53.29	<0.0001
A	396.95	1	396.95	241.80	<0.0001
B	242.25	1	242.25	147.57	<0.0001
C	90.52	1	90.52	55.14	0.0001
AB	4.83	1	4.83	2.94	0.1301
AC	23.11	1	23.11	14.08	0.0072
BC	7.91	1	7.91	4.82	0.0642
A ²	16.47	1	16.47	10.03	0.0158
B ²	2.59	1	2.59	1.58	0.2494
C ²	1.12	1	1.12	0.68	0.4364
Residual	11.49	7	1.64		
Lack of fit	7.55	3	2.52	2.55	0.1939
Pure error	3.95	4	0.99		
Corr. total	798.75	16			

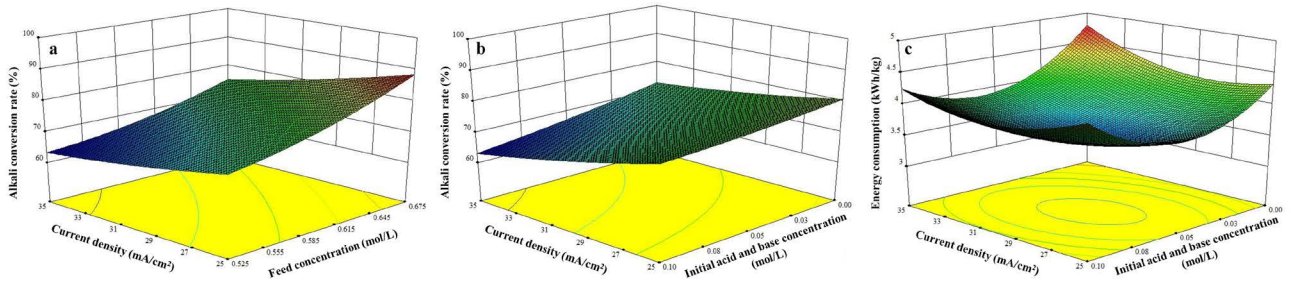


Fig. 6. 3D graphs of interactive effects. (a) Feed concentration and current density for alkali conversion rate, (b) current density and initial base concentration for alkali conversion rate, and (c) current density and initial base concentration for energy consumption.

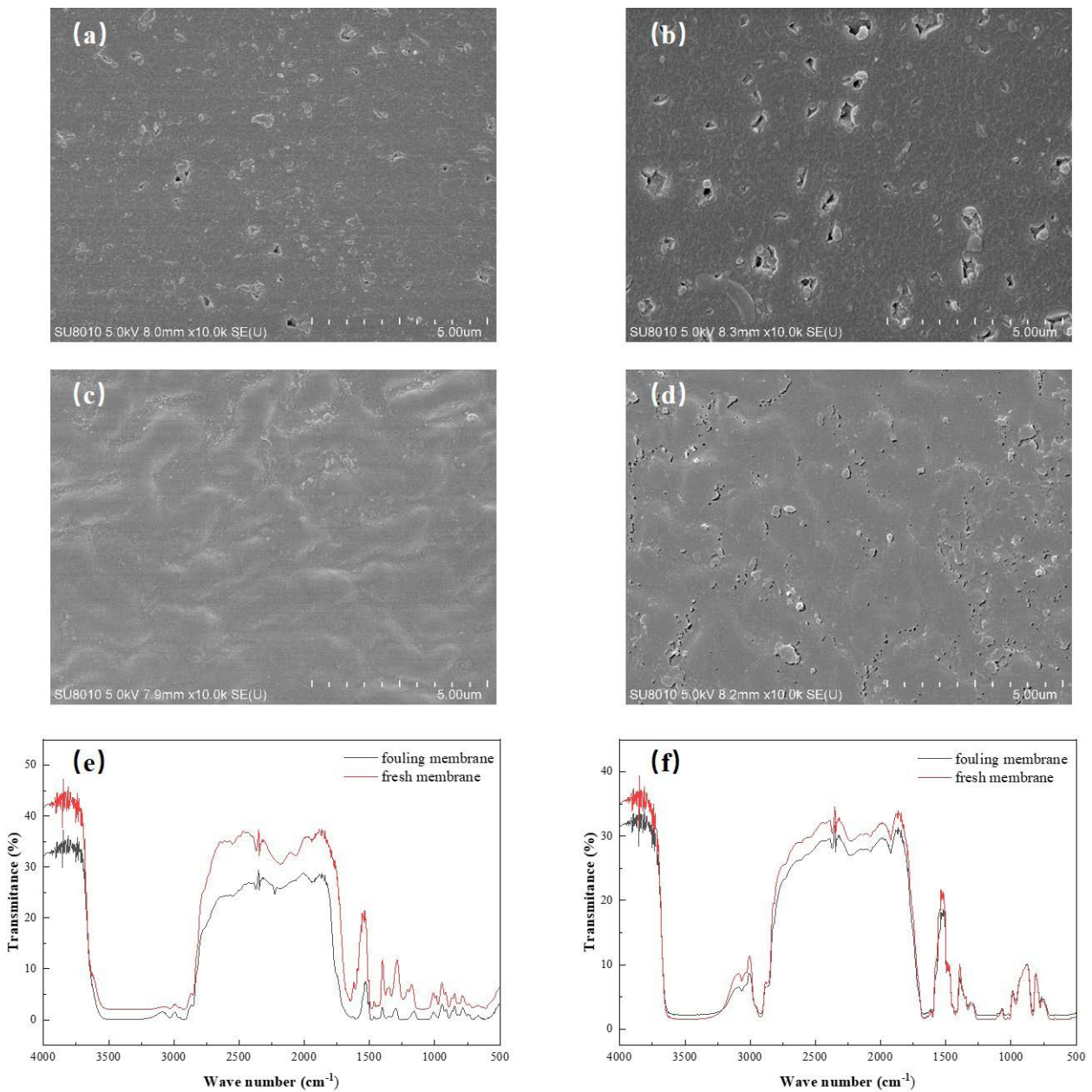


Fig. 7. SEM images and FTIR results of membranes, (a) fresh CEM, (b) fouling CEM, (c) fresh AEM, (d) fouling AEM, (e) FTIR results of CEM, and (f) FTIR results of AEM.

Table 4
Economic analysis of BMED process

Parameters	BMED process
Current density (mA/cm ²)	25
Feed concentration (mol/L)	0.675
Effective membrane area (cm ²)	189
Energy consumption (kWh/kg NaOH)	1.18
Electricity charge (\$/kWh)	0.10
Energy cost for regeneration (\$/kg NaOH)	0.12
Energy cost for peripheral equipment (\$/kg NaOH)	0.01
Total energy cost (\$/kg NaOH)	0.13
Membrane lifespan (y)	3
Peripheral equipment amortization period (y)	3
Membrane prices (\$/m ²)	1,100 (Bipolar membrane) 100 (Membrane)
Membrane cost (\$)	122.85
Stack cost (\$)	184.28
Peripheral equipment cost (\$)	276.42
Total investment cost (\$)	460.70
Amortization (\$/y)	153.57
Interest (\$/y)	36.86
Maintenance (\$/y)	46.07
Total fixed cost (\$/y)	236.50
Total process cost (\$/kg NaOH)	0.84

0.675 mol/L, current density 25 mA/cm² and initial acid and base concentration 0 mol/L. Under this condition, alkali conversion rate could be higher than 89.99%. The investment cost and energy consumption for producing base were \$236.50/y and \$0.13/kg, respectively. The process cost for the regeneration of 1kg NaOH from FGD wastewater was \$0.84.

Acknowledgements

The authors gratefully appreciate financial support provided by Department of Science and Technology of Jilin Province (20210203198SF) and Jilin Science and Technology Bureau Outstanding Young Talents Training Project (20200104114).

References

- [1] X. Liu, B. Lin, Y. Zhang, Sulfur dioxide emission reduction of power plants in China: current policies and implications, *J. Cleaner Prod.*, 113 (2016) 133–143.
- [2] S. Ma, J. Chai, G. Chen, W. Yu, S. Zhu, Research on desulfurization wastewater evaporation: present and future perspectives, *Renewable Sustainable Energy Rev.*, 58 (2016) 1143–1151.
- [3] Z. Liang, L. Zhang, Z. Yang, T. Qiang, G. Pu, J. Ran, Evaporation and crystallization of a droplet of desulfurization wastewater from a coal-fired power plant, *Appl. Therm. Eng.*, 119 (2017) 52–62.
- [4] M. Xia, C. Ye, K. Pi, D. Liu, A.R. Gerson, Ca removal and Mg recovery from flue gas desulfurization (FGD) wastewater by selective precipitation, *Water Sci. Technol.*, 76 (2017) 2842–2850.
- [5] Y. Xin, Z. Zhou, Q. Ming, D. Sun, J. Han, X. Ye, S. Dai, L.-M. Jiang, X. Zhao, Y. An, A two-stage desalination process for zero liquid discharge of flue gas desulfurization wastewater by chloride precipitation, *J. Hazard. Mater.*, 397 (2020) 122744, doi: 10.1016/j.jhazmat.2020.122744.
- [6] W. Dou, Z. Zhou, J. Ye, R. Huang, L.-M. Jiang, G. Chen, X. Fei, Reusing effluent of flue gas desulfurization wastewater treatment process as an economical calcium source for phosphorus removal, *Water Sci. Technol.*, 76 (2017) 1429–1435.
- [7] M. Yaqub, W. Lee, Zero-liquid discharge (ZLD) technology for resource recovery from wastewater: a review, *Sci. Total Environ.*, 681 (2019) 551–563.
- [8] X. Han, D. Zhang, J. Yan, S. Zhao, J. Liu, Process development of flue gas desulphurization wastewater treatment in coal-fired power plants towards zero liquid discharge: energetic, economic and environmental analyses, *J. Cleaner Prod.*, 261 (2020) 121144, doi: 10.1016/j.jclepro.2020.121144.
- [9] T. Tong, M. Elimelech, The global rise of zero liquid discharge for wastewater management: drivers, technologies, and future directions, *Environ. Sci. Technol.*, 50 (2016) 6846–6855.
- [10] Z. Sun, L. Yang, S. Chen, L. Bai, X. Wu, Promoting the removal of fine particles and zero discharge of desulfurization wastewater by spray-turbulent agglomeration, *Fuel*, 270 (2020) 117461, doi: 10.1016/j.fuel.2020.117461.
- [11] P.K. Giesbrecht, M.S. Freund, Recent advances in bipolar membrane design and applications, *Chem. Mater.*, 32 (2020) 8060–8090.
- [12] R. Pärnamäe, S. Mareev, V. Nikonenko, S. Melnikov, N. Sheldeshov, V. Zabolotskii, H.V.M. Hamelers, M. Tedesco, Bipolar membranes: a review on principles, latest developments, and applications, *J. Membr. Sci.*, 617 (2021) 118538, doi: 10.1016/j.memsci.2020.118538.
- [13] Y. Qiu, L. Yao, J. Li, M. Miao, A. Sotto, J. Shen, Integration of bipolar membrane electro dialysis with ion-exchange adsorption for high-quality H₃PO₂ recovery from NaH₂PO₂, *ACS Omega*, 4 (2019) 3983–3989.
- [14] K. Yan, X. Hang, J. Liu, J. Luo, Y. Wan, Preparation of hypophosphorous acid by bipolar membrane electro dialysis: process optimization and phosphorous acid minimization, *Ind. Eng. Chem. Res.*, 58 (2019) 21855–21863.
- [15] M. Herrero-Gonzalez, N. Admon, A. Dominguez-Ramos, R. Ibañez, Environmental sustainability assessment of seawater reverse osmosis brine valorization by means of electro dialysis with bipolar membranes, *Environ. Sci. Pollut. Res.*, 27 (2020) 1256–1266.
- [16] M. Herrero-Gonzalez, P. Diaz-Guridi, A. Dominguez-Ramos, A. Irabien, Highly concentrated HCl and NaOH from brines using electro dialysis with bipolar membranes, *Sep. Purif. Technol.*, 242 (2020) 116785, doi: 10.1016/j.seppur.2020.116785.
- [17] B. Chen, C. Jiang, Y. Wang, R. Fu, Selectrodialysis with bipolar membrane for the reclamation of concentrated brine from RO plant, *Desalination*, 442 (2018) 8–15.
- [18] Y. Berkessa, Q. Lang, B. Yan, S. Kuang, Anion exchange membrane organic fouling and mitigation in salt valorization process from high salinity textile wastewater by bipolar membrane electro dialysis, *Desalination*, 465 (2019) 94–103.
- [19] Y. Liu, X. Ke, H. Zhu, R. Chen, X. Chen, X. Zheng, Y. Jin, B. Van der Bruggen, Treatment of raffinate generated via copper ore hydrometallurgical processing using a bipolar membrane electro dialysis system, *Chem. Eng. J.*, 382 (2020) 122956, doi: 10.1016/j.cej.2019.122956.
- [20] M. Xia, C. Ye, R. Cao, H. Huang, An innovative beneficial reclamation of flue gas desulfurization brine using bipolar membrane electro dialysis technique, *Int. J. Electrochem. Sci.*, 13 (2018) 5382–5395.
- [21] X. Zhang, C. Ye, K. Pi, J. Huang, Sustainable treatment of desulfurization wastewater by ion exchange and bipolar membrane electro dialysis hybrid technology, *Sep. Purif. Technol.*, 211 (2019) 330–339.

- [22] L. Zhong, X. Jiang, R. Zhang, J. Shao, L. Chi, Y. Wang, J. Jia, D. Ying, Green utilization of the concentrated brine from two-stage membranes in coal chemical industry using electrodialysis with bipolar membrane, *Sep. Purif. Technol.*, 256 (2021) 117816, doi: 10.1016/j.seppur.2020.117816.
- [23] G. Jiang, H. Li, M. Xu, H. Ruan, Sustainable reverse osmosis, electrodialysis and bipolar membrane electrodialysis application for cold-rolling wastewater treatment in the steel industry, *J. Water Process Eng.*, 40 (2021) 101968, doi: 10.1016/j.jwpe.2021.101968.
- [24] Y. Wang, C. Huang, T. Xu, Optimization of electrodialysis with bipolar membranes by using response surface methodology, *J. Membr. Sci.*, 362 (2010) 249–254.
- [25] M. Wang, K. Wang, Y. Jia, Q. Ren, The reclamation of brine generated from desalination process by bipolar membrane electrodialysis, *J. Membr. Sci.*, 452 (2014) 54–61.
- [26] J. Shen, Z. Hou, C. Gao, Using bipolar membrane electrodialysis to synthesize di-quatary ammonium hydroxide and optimization design by response surface methodology, *Chin. J. Chem. Eng.*, 25 (2017) 1176–1181.
- [27] Y. Li, S. Shi, H. Cao, X. Wu, Bipolar membrane electrodialysis for generation of hydrochloric acid and ammonia from simulated ammonium chloride wastewater, *Water Res.*, 89 (2016) 201–209.
- [28] M. Reig, S. Casas, O. Gibert, C. Valderrama, Integration of nanofiltration and bipolar electrodialysis for valorization of seawater desalination brines: production of drinking and waste water treatment chemicals, *Desalination*, 382 (2016) 13–20.
- [29] H. Yan, W. Li, Y. Zhou, M. Irfan, In-situ combination of bipolar membrane electrodialysis with monovalent selective anion-exchange membrane for the valorization of mixed salts into relatively high-purity monoprotic and diprotic acids, *Membranes*, 10 (2020) 135, doi: 10.3390/membranes10060135.
- [30] L. Yao, Y. Qiu, Y. Zhao, C. Tang, A continuous mode operation of bipolar membrane electrodialysis (BMED) for the production of high-pure choline hydroxide from choline chloride, *Sep. Purif. Technol.*, 233 (2020) 116054, doi: 10.1016/j.seppur.2019.116054.
- [31] Y. Qiu, L. Yao, C. Tang, Y. Zhao, Integration of electrodialysis and electrodialysis with bipolar membrane to salt lake treatment for the production of lithium hydroxide, *Desalination*, 465 (2019) 1–12.
- [32] L. Gurreri, A. Tamburini, A. Cipollina, G. Micale, Electrodialysis applications in wastewater treatment for environmental protection and resources recovery: a systematic review on progress and perspectives, *Membranes*, 10 (2020) 146, doi: 10.3390/membranes10070146.
- [33] Y. Lv, H. Yan, B. Yang, C. Wu, Bipolar membrane electrodialysis for the recycling of ammonium chloride wastewater: membrane selection and process optimization, *Chem. Eng. Res. Des.*, 138 (2018) 105–115.
- [34] J. Kroupa, J. Kincl, J. Cakl, Recovery of H_2SO_4 and NaOH from Na_2SO_4 by electrodialysis with heterogeneous bipolar membrane, *Desal. Water. Treat.*, 56 (2015) 3238–3246.
- [35] L. Zhong, X. Jiang, R. Zhang, J. Shao, Green utilization of the concentrated brine from two-stage membranes in coal chemical industry using electrodialysis with bipolar membrane, *Sep. Purif. Technol.*, 256 (2021) 117816, doi: 10.1016/j.seppur.2020.117816.
- [36] Y. Wei, Y. Wang, X. Zhang, T. Xu, Comparative study on regenerating sodium hydroxide from the spent caustic by bipolar membrane electrodialysis (BMED) and electroelectrodialysis (EED), *Sep. Purif. Technol.*, 118 (2013) 1–5.
- [37] X. Wei, Y. Wang, H. Yan, C. Jiang, A sustainable valorization of neopentyl glycol salt waste containing sodium formate via bipolar membrane electrodialysis, *Sep. Purif. Technol.*, 254 (2021) 117563, doi: 10.1016/j.seppur.2020.117563.
- [38] S. Melnikov, S. Loza, M. Sharafan, V. Zabolotskiy, Electrodialysis treatment of secondary steam condensate obtained during production of ammonium nitrate. Technical and economic analysis, *Sep. Purif. Technol.*, 157 (2016) 179–191.
- [39] X. Gao, Y. Yang, L. Fu, Z. Sun, Regenerating spent acid produced by HZSM-5 zeolite preparation by bipolar membrane electrodialysis, *Sep. Purif. Technol.*, 125 (2014) 97–102.